CrossMark

JFM RAPIDS

Evaporation of multiple droplets

Hassan Masoud[1,†]**, Peter D. Howell**[2] **and Howard A. Stone**[3,†]

[1]Department of Mechanical Engineering-Engineering Mechanics, Michigan Technological University, Houghton, MI 49931, USA

[2]Mathematical Institute, University of Oxford, Oxford OX2 6GG, UK

[3]Department of Mechanical and Aerospace Engineering, Princeton University, Princeton, NJ 08544, USA

We derive an accurate estimate for the diffusive evaporation rates of multiple droplets of different sizes and arbitrary contact angles placed on a horizontal substrate. The derivation, which is based on a combination of Green's second identity and the method of reflections, simply makes use of the solution for the evaporation of a single droplet. The theoretical results can serve as a guide for future computational and experimental studies on the collective evaporation of arrays of droplets, as well as similar multi-body, diffusion-dominated transport problems.

Key words: drops, condensation/evaporation, contact lines

1. Introduction

The study of droplet evaporation on solid surfaces has a rich history in the field of transport phenomena (see e.g. Cazabat & Guena 2010; Erbil 2012; Stauber *et al.* 2014; Brutin & Starov 2018; Giorgiutti-Dauphiné & Pauchard 2018). While the majority of research has focused on the drying of single sessile droplets, there is broad interest in understanding the evaporation of multiple drops through experiments, simulations and theory; representative studies include Schäfle *et al.* (1999), Sokuler *et al.* (2010), Carrier *et al.* (2016), Shaikeea, Jyoti & Basu (2016), Laghezza *et al.* (2016), Castanet *et al.* (2016), Bao *et al.* (2018), Hatte *et al.* (2019), Chong *et al.* (2020) and Wray, Duffy & Wilson (2020). Among the most recent of these investigations is the theoretical analysis of Wray *et al.* (2020). Repurposing the mathematical derivation of Fabrikant (1985), they presented approximate expressions for the local and integrated evaporative flux from the surface of an array of thin (i.e. disk-like) droplets. The approximate total evaporation rates were then integrated in time to calculate the evolution and lifetime of the evaporating drops. The results of these calculations were subsequently compared with the experimental

† Email addresses for correspondence: hmasoud@mtu.edu, hastone@princeton.edu

measurements of Khilifi *et al.* (2019) involving seven droplets arranged in an I-shaped configuration.

Here, we provide a straightforward and physically insightful approach to obtain the evaporation rates of multiple droplets, which is not restricted to a particular geometry. This integral theorem-based approach and its possible extensions should be broadly useful as compared with more laborious methods that have been traditionally employed to study diffusive mass transfer problems involving two or more objects.

2. Problem statement and solution

Consider an array of droplets (all the same liquid, but possibly different sizes) numbered $n = 1, 2, \ldots, N$, with S_n denoting the free surface area of the n-th droplet (see figure 1). Let $\phi = (c - c_\infty) / (c_s - c_\infty)$ be the dimensionless vapour concentration field, where c is the dimensional concentration field, and c_s and c_∞ are its values on the free surface of the droplets and far away from them, respectively. In many practical situations, the time scale for the diffusion of the vapour concentration is much smaller than the total evaporation time of the droplets. For instance, for millimetre-sized water droplets drying in still air at room conditions, the ratio of these two time scales is very small (of the order of 10^{-5}). Moreover, for slowly evaporating drops under (nearly) isothermal conditions, the advective vapour transport by the Stefan and buoyancy-driven flows can be neglected. Therefore, assuming that the transport of the vapour phase is dominated by diffusion, we then have

$$\nabla^2 \phi = 0, \tag{2.1a}$$

with the boundary conditions

$$\phi = 1, \quad \text{on } S_1, S_2, \ldots, S_N, \quad \boldsymbol{n} \cdot \nabla \phi = 0, \quad \text{on } S_s, \quad \text{and} \quad \phi \to 0, \quad \text{as } r = |\boldsymbol{r}| \to \infty, \tag{2.1b}$$

where S_s represents the exposed surface of the substrate, $\boldsymbol{r}$ is the position vector and $\boldsymbol{n}$ is the unit normal vector directed into the vapour phase.

Our goal is to determine the rate at which the n-th droplet loses mass. This quantity, represented by J_n, is obtained by integrating the flux of c over S_n, i.e.

$$J_n = -\mathcal{D} (c_s - c_\infty) \int_{S_n} \boldsymbol{n} \cdot \nabla \phi \, \mathrm{d}S, \tag{2.2}$$

where $\mathcal{D}$ is the diffusion coefficient of the vapour. Conventionally, the evaporation rate is calculated after solving the boundary-value problem described by (2.1). However, for an array of droplets, as we now show, it is possible to construct an approximate expression for J_n without directly solving for ϕ.

### 2.1. *An integral-theorem-based representation of the net fluxes*

Consider the auxiliary field $\hat{\phi}_n$ corresponding to the evaporation of the n-th droplet in the absence of other drops. Here $\hat{\phi}_n$ satisfies

$$\nabla^2 \hat{\phi}_n = 0, \quad \text{with } \hat{\phi}_n = 1, \quad \text{on } S_n, \quad \boldsymbol{n} \cdot \nabla \hat{\phi}_n = 0, \quad \text{on } S_{\hat{s}} \quad \text{and}$$

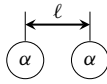$$\hat{\phi}_n \to 0, \quad \text{as } r \to \infty, \tag{2.3}$$

where $S_{\hat{s}}$ denotes the non-wetted area of the substrate. Next, apply Green's second identity (see e.g. Vandadi, Jafari Kang & Masoud 2016; Masoud & Stone 2019) between ϕ and $\hat{\phi}$

(*a*)
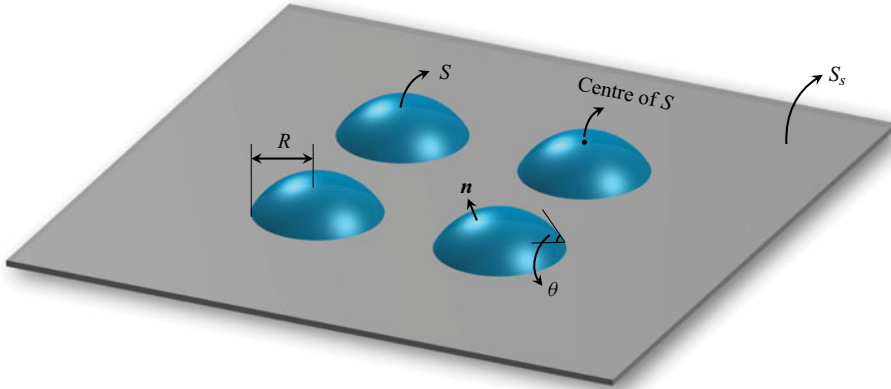
(*b*)

(*c*)

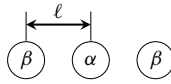
(*d*)
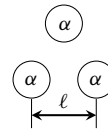
(*e*)
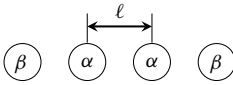
(*f*)
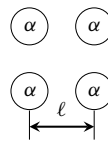
(*g*)
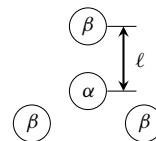
(*h*)
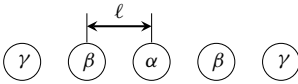
(*i*)
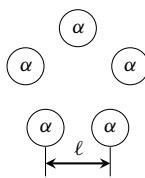
(*j*)
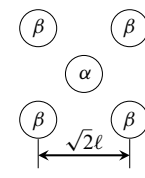
(*k*)
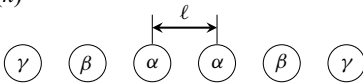
(*l*)
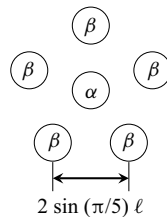
(*m*)
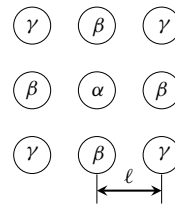
Figure 1. (*a*) Evaporation of four identical spherical-cap sessile droplets with contact radius R and contact angle θ, as an example of a multi-droplet problem described by (2.1). (*b*–*m*) Droplet arrangements considered in the validation study (see figure 2, and tables 1 and 2 of Appendix A). In each configuration, droplets with the same rate of evaporation are grouped together and labelled α, β or γ.

to arrive at

$$\int_{S_1+S_2+\cdots+S_N+S_s+S_\infty} \hat{\phi}\, \boldsymbol{n} \cdot \boldsymbol{\nabla}\phi \, \mathrm{d}S = \int_{S_1+S_2+\cdots+S_N+S_s+S_\infty} \phi\, \boldsymbol{n} \cdot \boldsymbol{\nabla}\hat{\phi} \, \mathrm{d}S, \qquad (2.4)$$

where S_∞ represents a bounding surface at infinity. Integrals over S_∞ vanish since both ϕ and $\hat{\phi}_n$ decay sufficiently fast at large distances. Integrals over the bare substrate are also zero because $\boldsymbol{n} \cdot \nabla \phi = \boldsymbol{n} \cdot \nabla \hat{\phi}_n = 0$ on S_s. Hence, we obtain

$$\int_{S_n} \hat{\phi}_n \, \boldsymbol{n} \cdot \nabla \phi \, \mathrm{d}S + \sum_{\substack{m=1, \\ m \neq n}}^{N} \int_{S_m} \hat{\phi}_n \, \boldsymbol{n} \cdot \nabla \phi \, \mathrm{d}S$$

$$= \int_{S_n} \phi \, \boldsymbol{n} \cdot \nabla \hat{\phi}_n \, \mathrm{d}S + \sum_{\substack{m=1, \\ m \neq n}}^{N} \int_{S_m} \phi \, \boldsymbol{n} \cdot \nabla \hat{\phi}_n \, \mathrm{d}S, \tag{2.5}$$

which further simplifies to

$$J_n - \mathcal{D} \, (c_s - c_\infty) \sum_{\substack{m=1, \\ m \neq n}}^{N} \int_{S_m} \hat{\phi}_n \, \boldsymbol{n} \cdot \nabla \phi \, \mathrm{d}S = \hat{J}_n \tag{2.6}$$

by using the boundary conditions in (2.1b) and (2.3), recalling the definitions of J and $\hat{J}$, and recognizing that $\int_S \boldsymbol{n} \cdot \nabla \hat{\phi}_n \, \mathrm{d}S = \int_V \nabla^2 \hat{\phi}_n \, \mathrm{d}V = 0$, where S is the surface enclosing the volume V located outside of the n-th droplet. Indeed, (2.6), which is an exact relation for the total flux from any drop n in an array of N drops, recovers Fabrikant's formula for the net flux of a potential flow through a perforated plate with arbitrarily distributed circular holes (Fabrikant 1985), which was obtained via a series of complex transformations (see also Wray *et al.* 2020).

2.2. *An approximation scheme for solving (2.6)*

To determine J_n, according to (2.6), we need to approximate the surface integrals over S_m. From the method of reflections, ϕ in the neighbourhood of the m-th droplet (i.e. near S_m) can be expressed as

$$\phi = \phi_m^{(0)} + \sum_{i=1}^{\infty} \left(\phi_m^{(i)} + \sum_{\substack{n=1, \\ n \neq m}}^{N} \phi_n^{(i-1)} \right), \tag{2.7}$$

where

$$\phi_m^{(0)} = \frac{J_m}{\hat{J}_m} \, \hat{\phi}_m \quad \text{and} \quad \phi_m^{(i)} = \sum_{\substack{n=1, \\ n \neq m}}^{N} \phi_m^{(i,n)}, \quad \text{for } i \geq 1, \tag{2.8}$$

with $\phi_m^{(i,n)}$ being the correction field in response to the non-uniform disturbances arising from $\phi_n^{(i-1)}$ (e.g. see Kim & Karrila 2005; Michelin, Guérin & Lauga 2018). Note that, by

927 R4-4

definition, the reflections make no contribution to the net flux from S_m, i.e.

$$\int_{S_m} \boldsymbol{n} \cdot \nabla \phi_m^{(i,n)} \, \mathrm{d}S = \int_{S_m} \boldsymbol{n} \cdot \nabla \phi_n^{(i-1)} \, \mathrm{d}S = 0, \quad \text{for } n \neq m \quad \text{and} \quad i \geq 1. \quad (2.9)$$

In the same neighbourhood, we can also write $\hat{\phi}_n(\boldsymbol{r})$ in the form of a Taylor series expansion about a judiciously chosen point $\boldsymbol{r}_m$ (located in or about droplet m) as

$$\hat{\phi}_n(\boldsymbol{r}) = \hat{\phi}_n\Big|_{\boldsymbol{r}=\boldsymbol{r}_m} + (\boldsymbol{r} - \boldsymbol{r}_m) \cdot \nabla \hat{\phi}_n\Big|_{\boldsymbol{r}=\boldsymbol{r}_m} + \tfrac{1}{2} (\boldsymbol{r} - \boldsymbol{r}_m)(\boldsymbol{r} - \boldsymbol{r}_m) : \nabla\nabla \hat{\phi}_n\Big|_{\boldsymbol{r}=\boldsymbol{r}_m} + \cdots. \quad (2.10)$$

Replacing $\hat{\phi}_n$ and ϕ in the surface integral of interest with their representations from (2.8) and (2.10), we can write the exact expression

$$\int_{S_m} \hat{\phi}_n \, \boldsymbol{n} \cdot \nabla \phi \, \mathrm{d}S = \hat{\phi}_n\Big|_{\boldsymbol{r}=\boldsymbol{r}_m} \int_{S_m} \boldsymbol{n} \cdot \nabla \phi_m^{(0)} \, \mathrm{d}S + \hat{\phi}_n\Big|_{\boldsymbol{r}=\boldsymbol{r}_m} \int_{S_m} \boldsymbol{n} \cdot \nabla (\phi - \phi_m^{(0)}) \mathrm{d}S$$
$$+ \int_{S_m} \left(\hat{\phi}_n - \hat{\phi}_n\Big|_{\boldsymbol{r}=\boldsymbol{r}_m} \right) \boldsymbol{n} \cdot \nabla \phi_m^{(0)} \, \mathrm{d}S + \int_{S_m} \left(\hat{\phi}_n - \hat{\phi}_n\Big|_{\boldsymbol{r}=\boldsymbol{r}_m} \right) \boldsymbol{n} \cdot \nabla (\phi)(\phi - \phi_m^{(0)}) \, \mathrm{d}S. \quad (2.11)$$

The first integral on the right-hand side of this relation is equal to $-J_m/[\mathcal{D}(c_s - c_\infty)]$, while the second integral is zero (see (2.9)). The third integral is nil, too, because

$$\phi_m^{(1,n)} = - \left(\phi_n^{(0)} - \phi_n^{(0)}\Big|_{\boldsymbol{r}=\boldsymbol{r}_m} \right) = -\frac{J_n}{\hat{J}_n} \left(\hat{\phi}_n - \hat{\phi}_n\Big|_{\boldsymbol{r}=\boldsymbol{r}_m} \right) \quad (2.12)$$

on S_m and, therefore,

$$\int_{S_m} \left(\hat{\phi}_n - \hat{\phi}_n\Big|_{\boldsymbol{r}=\boldsymbol{r}_m} \right) \boldsymbol{n} \cdot \nabla \phi_m^{(0)} \, \mathrm{d}S = -\frac{J_m \hat{J}_n}{\hat{J}_m J_n} \int_{S_m} \hat{\phi}_m \, \boldsymbol{n} \cdot \nabla \phi_m^{(1,n)} \, \mathrm{d}S = 0, \quad (2.13)$$

where the first equality in (2.13) results from Green's second identity, followed by the use of $\hat{\phi}_m = 1$ on S_m and (2.9). In taking the above steps, it is important to recall that $\phi_m^{(1,n)}$ is responsible for cancelling out spurious non-uniformities on S_m imposed by the first reflection from droplet n, i.e. from the field $\phi_n^{(0)} = (J_n/\hat{J}_n) \hat{\phi}_n$.

Finally, let $\varepsilon = R/\ell$, where R and ℓ denote, respectively, the characteristic length scale of the largest drop (if they differ in size) and the minimum centre-to-centre distance between droplet pairs. Since $\hat{\phi}$ decays, to the leading order, as $1/r$, we infer that both $\hat{\phi}_n - \hat{\phi}_n|_{\boldsymbol{r}=\boldsymbol{r}_m}$ and $\nabla(\phi - \phi_m^{(0)})$ scale with ε^2, which means that the fourth integral in (2.11) scales with ε^4. Equation (2.11), therefore, reduces to

$$\int_{S_m} \hat{\phi}_n \, \boldsymbol{n} \cdot \nabla \phi \, \mathrm{d}S = -\frac{\hat{\phi}_n\Big|_{\boldsymbol{r}=\boldsymbol{r}_m} J_m}{\mathcal{D}(c_s - c_\infty)} + O(\varepsilon^4), \quad (2.14)$$

which, upon substitution in (2.6), yields

$$1 \approx \frac{J_n}{\hat{J}_n} + \sum_{\substack{m=1, \\ m \neq n}}^{N} \hat{\phi}_n\Big|_{\boldsymbol{r}=\boldsymbol{r}_m} \frac{J_m}{\hat{J}_n}. \quad (2.15)$$

The above expression constitutes a linear system of algebraic equations for J_n that can be readily solved provided that the solution of the single-droplet problem $\hat{\phi}$ (see (2.3))

is known. Thus, we have constructed an approximate formula for the evaporation rates of an array of multiple sessile droplets, even when the array contains a mixture of drops with different sizes and contact angles. We note that (2.15) recovers (3.2) of Wray *et al.* (2020) (which is identical to equation (15) of Fabrikant 1985) for the special case of disk-shaped (zero-thickness) droplets with r_m located at the centre of the disks. Perhaps more interestingly, (2.15) can also be viewed as a condition that enforces $\phi = 1$ on S_n during successive reflections (see e.g. Michelin *et al.* 2018).

2.3. *On the choice of the evaluation point r_m*

The accuracy of (2.15) beyond $O(\varepsilon)$ is dependent on the choice of the location of r_m. On one hand, the conventional wisdom suggests that we set the evaluation point of the Taylor series expansion to an origin about which the multipole expansion of $\hat{\phi}$ has no dipolar term. In the context of conduction heat transfer, this point is known as the 'centre of heat' (see e.g. Brenner 1963). For example, the heat centre for spherical-cap droplets is located at the centre of their contact area. However, on the other hand, we know that $\hat{\phi}$ is continuous and $n \cdot \nabla \phi$ is an integrable function that does not change sign on S_m. As a result, the mean value theorem for definite integrals argues for selecting a spot on the free surface of the droplet as the reference point for approximating the surface integrals in (2.6). Following this argument, as a generic approach (without extra fine-tuning), we choose the point of evaluation to be the geometric centre of S_m.

3. Discussion

To evaluate the fidelity of (2.15) with our choice of r_m, we compare its predictions for several test cases with the results obtained from the direct numerical solution of (2.1). Specifically, the comparisons are made for the evaporation of multiple identical spherical-cap droplets that are arranged in various configurations as depicted in figure 1(*b–m*). There exists an analytical solution for the evaporation of a single spherical-cap droplet with contact radius R, contact angle θ and free surface S (see e.g. Lebedev 1965; Popov 2005). From this solution (which was originally expressed in a boundary-fitting toroidal coordinate system), the distribution of the dimensionless vapour concentration field takes the form of

$$\hat{\phi} = 4A\frac{R}{\tilde{r}} + (A - 4B)\frac{R^3\left(\tilde{r}^2 - 3\tilde{z}^2\right)}{\tilde{r}^5} + O\left[\left(\frac{R}{\tilde{r}}\right)^5\right], \tag{3.1}$$

where

$$A = \frac{1}{8\pi R}\int_S n \cdot \nabla\hat{\phi}\,\mathrm{d}S = \int_0^\infty \left\{1 + \frac{\cosh\left[(2\pi - \theta)\,\tau\right]}{\cosh\left(\theta\tau\right)}\right\}^{-1}\,\mathrm{d}\tau, \tag{3.2a}$$

$$B = \int_0^\infty \left\{1 + \frac{\cosh\left[(2\pi - \theta)\,\tau\right]}{\cosh\left(\theta\tau\right)}\right\}^{-1}\tau^2\,\mathrm{d}\tau, \tag{3.2b}$$

$\tilde{r} = |\tilde{r}|$ and $\tilde{r} = r - r_c$ with r_c being the location of the centre of the droplet's contact area. Equation (3.1) offers an excellent approximation of $\hat{\phi}$ for $\tilde{r}/R \gtrsim 2$ (touching drops), and therefore it is used to calculate $\hat{\phi}_n|_{r=r_m}$ in (2.15). Note that the general form of the expansion for $\hat{\phi}$ is correct for any axisymmetric droplet. Of course, the formulae for A
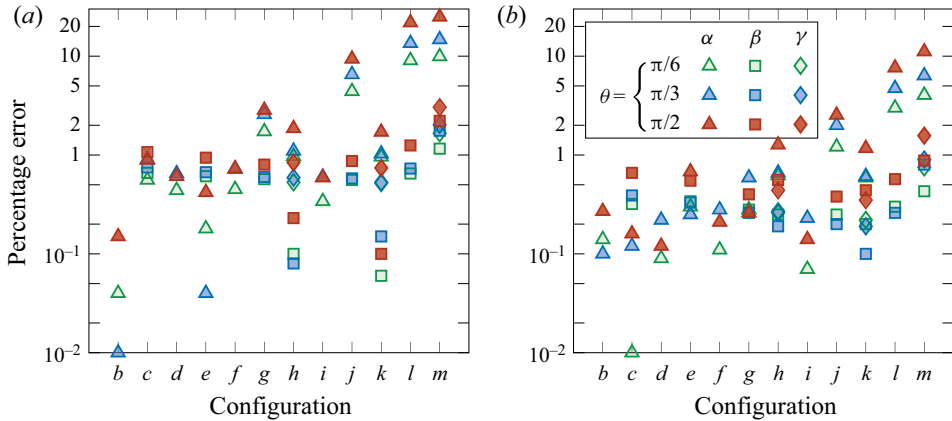
Figure 2. Percentage difference between the predictions of (2.15) (using (3.1)) for the normalized rates of evaporation and the results of the numerical simulations. The rates are normalized by their respective values for isolated (but otherwise the same) droplets, and are tabulated in tables 1 and 2 of Appendix A. The errors are calculated for the spacings (a) $\ell = 2.5R$ and (b) $\ell = 3R$ (see figure 1) and for the contact angles $\theta = \pi/6, \pi/3, \pi/2$. In each configuration, droplets with distinguished evaporation rates are labelled α, β and γ, as shown in figures 1(b–m).

and B differ from (3.2) for non-spherical-cap shapes. Furthermore, the leading-order (i.e. $O(R/\tilde{r})$) term in the expansion is valid for arbitrary geometries, with A being dependent on the specific shape.

In addition, a finite-element approach, as implemented in COMSOL Multiphysics, is employed to carry out the numerical calculations based on (2.1) and (2.1b). The outer boundary at infinity is modelled as a large hemisphere of radius $500R$, whose centre coincides with the centre of the droplet arrangements. Tetrahedral elements are used to mesh the computational domain such that the grid density is the highest in the vicinity of the droplets. The accuracy of the computational scheme was validated via comparison with highly accurate numerical results for the evaporation of a pair of identical disks (see table 1 of Fabrikant 1985). Specifically, we found that the relative error of our calculations for $J/\hat{J}$ is less than 0.3 % for all tabulated spacings ranging from $\ell = 2R$ to $\ell = 10R$.

We calculated the percentage difference between the predictions of (2.15) (using (3.1)) for the normalized rates of evaporation and those calculated numerically; the results are shown in figure 2. The rates are normalized by their respective values for an isolated (but otherwise the same) droplet, and their magnitudes are tabulated in tables 1 and 2 of Appendix A. The comparisons are made for two centre-to-centre droplet spacings of $\ell = 2.5R$ and $\ell = 3R$ (see figure 1), and three contact angles $\theta = \pi/6, \pi/3, \pi/2$. Note that, in each configuration, there may be one, two or three sets of droplets with distinguished evaporation rates. These sets are labelled α, β and γ (as shown in figure 1b–m) to facilitate the presentation of the results.

Inspecting the results, we find that the approximation error of (2.15) is only a few per cent or less for most cases. It appears, however, that our formulation underestimates the rate of evaporation for high-contact angle droplets that are surrounded by their neighbours (see the red triangles of configurations g, j, l and m). However, even in these cases, the maximum error is roughly 25 % for $\ell = 2.5R$ (red triangle of configuration m in figure 2a), which sharply declines to approximately 10 % as the spacing increases to $\ell = 3R$ (red triangle of configuration m in figure 2b). We also checked that had we set $\mathbf{r}_m$ to the contact area centre of the droplets (i.e. their centre of heat), the corresponding errors

Config.	θ	Numerical simulation			Prediction of (2.15) (using (3.1))			Estimation error (%)		
		α	β	γ	α	β	γ	α	β	γ
b	$\pi/6$	0.777	—	—	0.778	—	—	0.041	—	—
b	$\pi/3$	0.758	—	—	0.758	—	—	0.008	—	—
b	$\pi/2$	0.728	—	—	0.729	—	—	0.154	—	—
c	$\pi/6$	0.586	0.726	—	0.583	0.730	—	0.557	0.664	—
c	$\pi/3$	0.551	0.706	—	0.546	0.711	—	0.914	0.751	—
c	$\pi/2$	0.497	0.676	—	0.493	0.683	—	0.865	1.069	—
d	$\pi/6$	0.639	—	—	0.636	—	—	0.440	—	—
d	$\pi/3$	0.614	—	—	0.610	—	—	0.653	—	—
d	$\pi/2$	0.577	—	—	0.574	—	—	0.612	—	—
e	$\pi/6$	0.544	0.697	—	0.545	0.702	—	0.180	0.614	—
e	$\pi/3$	0.509	0.677	—	0.509	0.682	—	0.039	0.673	—
e	$\pi/2$	0.457	0.647	—	0.459	0.653	—	0.417	0.942	—
f	$\pi/6$	0.567	—	—	0.564	—	—	0.452	—	—
f	$\pi/3$	0.539	—	—	0.536	—	—	0.717	—	—
f	$\pi/2$	0.500	—	—	0.496	—	—	0.731	—	—
g	$\pi/6$	0.441	0.657	—	0.434	0.660	—	1.729	0.566	—
g	$\pi/3$	0.398	0.634	—	0.388	0.638	—	2.575	0.602	—
g	$\pi/2$	0.334	0.602	—	0.324	0.607	—	2.854	0.801	—
h	$\pi/6$	0.504	0.521	0.678	0.509	0.522	0.682	0.965	0.1	0.529
h	$\pi/3$	0.470	0.487	0.658	0.475	0.487	0.662	1.096	0.083	0.585
h	$\pi/2$	0.419	0.436	0.628	0.427	0.437	0.633	1.857	0.226	0.836
i	$\pi/6$	0.522	—	—	0.520	—	—	0.339	—	—
i	$\pi/3$	0.494	—	—	0.491	—	—	0.601	—	—
i	$\pi/2$	0.453	—	—	0.450	—	—	0.595	—	—
j	$\pi/6$	0.343	0.584	—	0.328	0.588	—	4.413	0.559	—
j	$\pi/3$	0.299	0.56	—	0.280	0.563	—	6.540	0.584	—
j	$\pi/2$	0.237	0.524	—	0.214	0.529	—	9.385	0.865	—
k	$\pi/6$	0.483	0.506	0.664	0.488	0.507	0.667	0.959	0.056	0.517
k	$\pi/3$	0.449	0.472	0.644	0.454	0.472	0.647	1.029	0.153	0.527
k	$\pi/2$	0.400	0.422	0.614	0.406	0.422	0.618	1.707	0.099	0.737
l	$\pi/6$	0.282	0.517	—	0.257	0.520	—	9.054	0.648	—
l	$\pi/3$	0.241	0.491	—	0.209	0.495	—	13.507	0.732	—
l	$\pi/2$	0.186	0.454	—	0.146	0.460	—	21.873	1.246	—
m	$\pi/6$	0.234	0.355	0.476	0.211	0.351	0.484	9.928	1.161	1.660
m	$\pi/3$	0.200	0.325	0.453	0.171	0.319	0.463	14.750	1.760	2.024
m	$\pi/2$	0.155	0.283	0.422	0.116	0.276	0.434	24.982	2.217	3.039

Table 1. Normalized evaporation rates of multiple identical spherical-cap droplets (with contact radius R and contact angle θ) arranged in various configurations as shown in figure 1(*b–m*) of the main text. The rates are normalized by their respective values for a single (but otherwise the same) droplet. The results are reported for the spacing $\ell = 2.5R$ and contact angles $\theta = \pi/6, \pi/3, \pi/2$.

would have been much larger, nearly 40 % and 20 % errors, respectively. The relatively higher prediction errors are partly due to stronger shielding effects in the aforementioned configurations, which significantly decrease the evaporation rate of the α-type droplets. To put this into perspective, the evaporation rate for the middle droplet in configuration m when its contact angle is $\theta = \pi/2$ is reduced to approximately 15 % of the rate at which the same droplet evaporates in isolation. Overall, the results of figure 2 demonstrate the high fidelity of the evaporation rates predicted by (2.15). We reiterate that the predictions here, for a wide range of configurations, are obtained using only the solution of the single-droplet problem and solving a linear system of algebraic equations (see (2.15) and (3.1)).

Config.	θ	Numerical simulation			Prediction of (2.15) (using (3.1))			Estimation error (%)		
		α	β	γ	α	β	γ	α	β	γ
b	$\pi/6$	0.807	—	—	0.808	—	—	0.136	—	—
b	$\pi/3$	0.788	—	—	0.789	—	—	0.101	—	—
b	$\pi/2$	0.758	—	—	0.760	—	—	0.273	—	—
c	$\pi/6$	0.640	0.757	—	0.640	0.759	—	0.014	0.321	—
c	$\pi/3$	0.605	0.736	—	0.605	0.739	—	0.120	0.391	—
c	$\pi/2$	0.551	0.704	—	0.552	0.709	—	0.157	0.662	—
d	$\pi/6$	0.679	—	—	0.678	—	—	0.088	—	—
d	$\pi/3$	0.653	—	—	0.651	—	—	0.218	—	—
d	$\pi/2$	0.613	—	—	0.613	—	—	0.119	—	—
e	$\pi/6$	0.597	0.728	—	0.599	0.731	—	0.297	0.335	—
e	$\pi/3$	0.562	0.707	—	0.564	0.709	—	0.253	0.332	—
e	$\pi/2$	0.508	0.675	—	0.512	0.679	—	0.677	0.554	—
f	$\pi/6$	0.610	—	—	0.610	—	—	0.108	—	—
f	$\pi/3$	0.581	—	—	0.580	—	—	0.283	—	—
f	$\pi/2$	0.538	—	—	0.537	—	—	0.206	—	—
g	$\pi/6$	0.510	0.690	—	0.508	0.692	—	0.284	0.285	—
g	$\pi/3$	0.466	0.667	—	0.464	0.668	—	0.590	0.258	—
g	$\pi/2$	0.399	0.632	—	0.398	0.634	—	0.260	0.405	—
h	$\pi/6$	0.557	0.574	0.709	0.560	0.575	0.711	0.624	0.253	0.270
h	$\pi/3$	0.522	0.539	0.688	0.525	0.540	0.690	0.662	0.185	0.260
h	$\pi/2$	0.468	0.486	0.656	0.474	0.489	0.659	1.271	0.558	0.442
i	$\pi/6$	0.567	—	—	0.567	—	—	0.071	—	—
i	$\pi/3$	0.537	—	—	0.535	—	—	0.232	—	—
i	$\pi/2$	0.492	—	—	0.491	—	—	0.141	—	—
j	$\pi/6$	0.415	0.621	—	0.410	0.622	—	1.206	0.246	—
j	$\pi/3$	0.369	0.595	—	0.362	0.596	—	2.001	0.198	—
j	$\pi/2$	0.301	0.557	—	0.293	0.559	—	2.542	0.378	—
k	$\pi/6$	0.535	0.559	0.695	0.538	0.560	0.697	0.594	0.201	0.220
k	$\pi/3$	0.500	0.524	0.674	0.503	0.524	0.675	0.611	0.102	0.186
k	$\pi/2$	0.447	0.471	0.642	0.453	0.473	0.644	1.165	0.442	0.352
l	$\pi/6$	0.350	0.556	—	0.339	0.558	—	3.004	0.296	—
l	$\pi/3$	0.305	0.529	—	0.291	0.530	—	4.733	0.261	—
l	$\pi/2$	0.241	0.489	—	0.223	0.492	—	7.626	0.569	—
m	$\pi/6$	0.288	0.403	0.512	0.276	0.401	0.516	4.035	0.430	0.748
m	$\pi/3$	0.249	0.370	0.487	0.233	0.367	0.492	6.360	0.801	0.904
m	$\pi/2$	0.196	0.323	0.452	0.174	0.320	0.459	11.131	0.885	1.565

Table 2. Normalized evaporation rates of multiple identical spherical-cap droplets (with contact radius R and contact angle θ) arranged in various configurations as shown in figures 1(*b–m*) of the main text. The rates are normalized by their respective values for a single (but otherwise the same) droplet. The results are reported for the spacing $\ell = 3R$ and contact angles $\theta = \pi/6, \pi/3, \pi/2$.

In conclusion, we highlight that the implications of our findings go beyond the evaporation of sessile droplets and extend to a large class of diffusive mass transfer problems that also includes, among other problems, the dissolution of micro and nano bubbles (see e.g. Dollet & Lohse 2016; Michelin *et al.* 2018; Zhu *et al.* 2018). Additional areas of physics that benefit from our solution strategy for the Laplace equation are potential flow, conduction heat transfer, electrostatics, etc. Moreover, we note that our derivations can be further generalized, often in a fairly straightforward fashion, to include, for example, (i) pendent drops of unequal size, (ii) transient effects, (iii) additional linear terms in the governing equation (e.g. solving for the Helmholtz rather than the Laplace equation) and (iv) Neumann or mixed (Robin) boundary conditions on S_n.

Author ORCIDs.
Hassan Masoud https://orcid.org/0000-0001-8932-3479;
Peter D. Howell https://orcid.org/0000-0002-6036-3386;
Howard A. Stone https://orcid.org/0000-0002-9670-0639.

Appendix A. Tabulated evaporation rates

The evaporation rates corresponding to figures 2(*a*) and 2(*b*) are presented in tables 1 and 2, respectively. The rates are given in a normalized form, i.e. they are divided by their respective values for a single (but otherwise the same) droplet. We note that the evaporation rate of an isolated sessile droplet can be calculated from (3.2*a*), and the specific values for drops with contact angles $\theta = \pi/6, \pi/3, \pi/2$ are, respectively,

$$\hat{J}_{\pi/6} = 4.416, \quad \hat{J}_{\pi/3} = 5.086 \quad \text{and} \quad \hat{J}_{\pi/2} = 2\pi, \qquad (\text{A1}a\text{--}c)$$

where $\hat{J}$ is non-dimensionalized by $\mathcal{D}R\,(c_s - c_\infty)$.

REFERENCES

BAO, L., SPANDAN, V., YANG, Y., DYETT, B., VERZICCO, R., LOHSE, D. & ZHANG, X. 2018 Flow-induced dissolution of femtoliter surface droplet arrays. *Lab Chip* **18** (7), 1066–1074.

BRENNER, H. 1963 Forced convection heat and mass transfer at small Peclet numbers from a particle of arbitrary shape. *Chem. Engng Sci.* **18** (2), 109–122.

BRUTIN, D. & STAROV, V. 2018 Recent advances in droplet wetting and evaporation. *Chem. Soc. Rev.* **47** (2), 558–585.

CARRIER, O., SHAHIDZADEH-BONN, N., ZARGAR, R., AYTOUNA, M., HABIBI, M., EGGERS, J. & BONN, D. 2016 Evaporation of water: evaporation rate and collective effects. *J. Fluid Mech.* **798**, 774–786.

CASTANET, G., PERRIN, L., CABALLINA, O. & LEMOINE, F. 2016 Evaporation of closely-spaced interacting droplets arranged in a single row. *Intl J. Heat Mass Transfer* **93**, 788–802.

CAZABAT, A.-M. & GUENA, G. 2010 Evaporation of macroscopic sessile droplets. *Soft Matt.* **6** (12), 2591–2612.

CHONG, K.L., LI, Y., NG, C.S., VERZICCO, R. & LOHSE, D. 2020 Convection-dominated dissolution for single and multiple immersed sessile droplets. *J. Fluid Mech.* **892**, A21.

DOLLET, B. & LOHSE, D. 2016 Pinning stabilizes neighboring surface nanobubbles against Ostwald ripening. *Langmuir* **32** (43), 11335–11339.

ERBIL, H.Y. 2012 Evaporation of pure liquid sessile and spherical suspended drops: a review. *Adv. Colloid Interface Sci.* **170** (1-2), 67–86.

FABRIKANT, V.I. 1985 On the potential flow through membranes. *Z. Angew. Math. Phys.* **36** (4), 616–623.

GIORGIUTTI-DAUPHINÉ, F. & PAUCHARD, L. 2018 Drying drops. *Eur. Phys. J.* E **41** (3), 32.

HATTE, S., PANDEY, K., PANDEY, K., CHAKRABORTY, S. & BASU, S. 2019 Universal evaporation dynamics of ordered arrays of sessile droplets. *J. Fluid Mech.* **866**, 61–81.

KHILIFI, D., FOUDHIL, W., FAHEM, K., HARMAND, S. & BEN, J.S. 2019 Study of the phenomenon of the interaction between sessile drops during evaporation. *Therm. Sci.* **23** (2B), 1105–1114.

KIM, S. & KARILLA, S.J. 2005 *Microhydrodynamics: Principles and Selected Applications*. Dove.

LAGHEZZA, G., DIETRICH, E., YEOMANS, J.M., LEDESMA-AGUILAR, R., KOOIJ, E.S., ZANDVLIET, H.J.W. & LOHSE, D. 2016 Collective and convective effects compete in patterns of dissolving surface droplets. *Soft Matt.* **12** (26), 5787–5796.

LEBEDEV, N.N. 1965 *Special Functions and Their Applications*. Prentice-Hall.

MASOUD, H. & STONE, H.A. 2019 The reciprocal theorem in fluid dynamics and transport phenomena. *J. Fluid Mech.* **879**, P1.

MICHELIN, S., GUÉRIN, E. & LAUGA, E. 2018 Collective dissolution of microbubbles. *Phys. Rev. Fluids* **3** (4), 043601.

POPOV, Y.O. 2005 Evaporative deposition patterns: spatial dimensions of the deposit. *Phys. Rev. E* **71** (3), 036313.

SCHÄFLE, C., BECHINGER, C., RINN, B., DAVID, C. & LEIDERER, P. 1999 Cooperative evaporation in ordered arrays of volatile droplets. *Phys. Rev. Lett.* **83** (25), 5302.

SHAIKEEA, A., JYOTI, D. & BASU, S. 2016 Insight into the evaporation dynamics of a pair of sessile droplets on a hydrophobic substrate. *Langmuir* **32** (5), 1309–1318.

SOKULER, M., AUERNHAMMER, G.K., LIU, C.J., BONACCURSO, E. & BUTT, H.-J. 2010 Dynamics of condensation and evaporation: effect of inter-drop spacing. *Europhys. Lett.* **89** (3), 36004.

STAUBER, J.M., WILSON, S.K., DUFFY, B.R. & SEFIANE, K. 2014 On the lifetimes of evaporating droplets. *J. Fluid Mech.* **744**, R2.

VANDADI, V., JAFARI KANG, S. & MASOUD, H. 2016 Reciprocal theorem for convective heat and mass transfer from a particle in Stokes and potential flows. *Phys. Rev. Fluids* **1** (2), 022001.

WRAY, A.W., DUFFY, B.R & WILSON, S.K. 2020 Competitive evaporation of multiple sessile droplets. *J. Fluid Mech.* **884**, A45.

ZHU, X., VERZICCO, R., ZHANG, X. & LOHSE, D. 2018 Diffusive interaction of multiple surface nanobubbles: shrinkage, growth, and coarsening. *Soft Matt.* **14** (11), 2006–2014.